Motion Compensation in Six Degrees of Freedom for a MIMO Radar Mounted on a Hovering UAV

Philipp Stockel, Patrick Wallrath, Reinhold Herschel, Nils Pohl

Abstract

This paper deals with the motion of a hovering UAV with six degrees of freedom. The effects of the motion on the measured signal of a MIMO radar mounted underneath the UAV are analyzed. For each degree of freedom, namely the translation in x-, y- and z-direction as well as the rotation around x-, y- and z-axis, an algorithm is proposed to compensate the considered motion. The effectiveness of the proposed algorithms is demonstrated by measuring validated vital signs independent of the current UAV motion.

Index Terms

MIMO radar, unmanned arial vehicle (UAV), FMCW radar, radar detection, vital signs, motion compensation, inertial measurement unit (IMU)

I. Introduction

FOR critical scenarios in civil or military context in which missing people should be detected but the involvement of humans is dangerous, unmanned aerial vehicles (UAV) offer promising possibilities. In this context, the use of a Multiple Input Multiple Output (MIMO) radar system mounted underneath a UAV enables the localization of humans and furthermore the evaluation of their vital signs. Unfortunately, the motion of the UAV interferes with the motion of the targets. This makes the direct detection of dynamic targets as well as the evaluation of their motion impossible. Therefore, the motion of the UAV has to be compensated.

There are already different approaches to compensate the vertical motion of the UAV. They are based on measuring the distance to the floor with an additional measuring system [1][2] or by evaluating the voxel with the strongest reflection for a MIMO radar [3]. These approaches will be problematic if the target lies directly in the focus of the radar system. In all the mentioned publications the compensation of horizontal vibrations as well as the compensation of rotations around the three axes is not considered at all.

In this paper, we analyze the effects of the motion in six degrees of freedom namely the translation in x-, y- and z-direction as well as the rotation around the x-, y- and z-axis. We focus on the hovering scenario, which means that the translational motions are limited to vibrations. Furthermore, we propose algorithms to compensate the effects of the six motions. Therefore, we use information measured by an Inertial Measurement Unit (IMU) mounted on the UAV as well as information measured by the radar itself. We start by introducing the scenario, the radar system and the IMU. Then, the different motions are analyzed one by one and the corresponding compensation techniques are proposed. Finally, we show our measured results.

P. Stockel, P. Wallrath, R. Herschel and N. Pohl are with the Fraunhofer Institute for High Frequency Physics and Radar Techniques, Wachtberg, Germany

P. Stockel, P. Wallrath, and N. Pohl are with the Institute for Integrated Systems, Ruhr-University Bochum, Bochum, Germany

e-mail: philipp.stockel@fhr.fraunhofer.de

II. Scenario Description

The basic scenario consists of a UAV equipped with a MIMO radar and an IMU. We assume that the approximate position of the human target is known, so that the UAV can fly to the coarse position of the target and hover there. Locating the approximate position can be done with the radar itself or with other sensors, but that is beyond the scope of this publication [4]. While hovering, the system tries to find the exact position of the person. To ensure that the person is detectable in the radar data, the considered azimuth and elevation angles are restricted to values smaller than $\pm 40°$. After locating a person, their motion and the vital signs are extracted. To enable this, the motion of the UAV has to be minimal. Since it is impossible to ensure the immobility of the radar by mechanical techniques or by regulating the rotors, we have to compensate the motion by signal processing. For the remainder of this publication, the z-axis represents the vertical axis going directly through the center of the radar antenna topology and the UAV. Consequently, the x- and y-axis form the horizontal plane.

A. Radar Signal Processing

The virtual array of the used FMCW[1] MIMO radar should be two-dimensional so that both the azimuth angle and the elevation angle of a target can be evaluated. The radar signal $g(m_{\text{chirp}}, m_{\text{x}}, m_{\text{y}}, t)$ describes the $m_{\text{chirp}}^{\text{th}}$ chirp sample of the antenna element with the index $(m_{\text{x}}, m_{\text{y}})$ in the virtual array belonging to the frame with time index t, where $m_{\text{chirp}} = 1, ..., M_{\text{chirp}}$, $m_{\text{x}} = 1, ..., M_{\text{x}}$, $m_{\text{y}} = 1, ..., M_{\text{y}}$ and $t = 0, ..., T$. If we calculate the Fourier transform in the first dimension or more precisely over the samples of the chirps, we will get $G(r, m_{\text{x}}, m_{\text{y}}, t)$. The variable r describes the range the signal is corresponding to. If also the Fourier transform in the second and third dimension is calculated, it will result

[1]Frequency modulated continuous wave

in $f(r, \Phi, \Theta, t)$ where Φ and Θ define the azimuth and the elevation angle from which the signal $f(r, \Phi, \Theta, t)$ is coming [5]. One element $f(r, \Phi, \Theta, t)$ is also called voxel because the signal corresponds to a specified position in the three-dimensional space. The evaluation of the signal from a target located in the voxel $(r_\mathrm{h}, \Phi_\mathrm{h}, \Theta_\mathrm{h})$ over time results in the slow time signal

$$s(t) = f(r_\mathrm{h}, \Phi_\mathrm{h}, \Theta_\mathrm{h}, t) = a(t) \exp(\mathrm{i} \cdot \phi(t)), \tag{1}$$

where $a(t)$ is the amplitude of the complex signal and $\phi(t)$ the phase [6].

If we look at a representation of all samples in the first two dimensions of $f(r, \Phi, \Theta, t)$, or rather all samples in range and azimuth for a given elevation angle and time step, we will call this in the following Range-Azimuth (RA) map. Similarly, the same depiction for the first and third or second and third dimension is called Range-Elevation (RE) or Azimuth-Elevation (AE) map, respectively. The calculation of the Doppler velocities by executing the Fourier transform over the time steps results in $F(r, \Phi, \Theta, v)$. If we depict the first and the fourth dimension of $F(r, \Phi, \Theta, v)$, we will obtain the Range-Doppler (RD) map [7].

B. Processing of the IMU Data

To get information about the motion of the radar system, we use the data measured by an IMU. The IMU should be mounted as close to the radar as possible. This ensures that the radar and the IMU are subjected to the same forces. In particular, the radar and the IMU should rotate around the same z-axis. Hence, the optimal position for the IMU would be directly above the radar.

The IMU contains three accelerometers measuring the acceleration in x-, y- and z-direction and three gyroscopes measuring the angular velocity in those directions or more precisely the nick, roll and yaw angular velocity. By combining the sensors, we can calculate an estimate of the position and orientation in the three-dimensional space. The sampling frequency of the IMU should be at least 100 Hz in order to calculate an accurate position.

To estimate the motion of the radar system using the IMU, we have to determine the orientation of the system. This is done by integrating the angular velocities measured by the gyroscope. The resulting data

$$\xi_\mathrm{IMU}(t) = \begin{pmatrix} \alpha_\mathrm{IMU}(t) \\ \beta_\mathrm{IMU} t \\ \gamma_\mathrm{IMU}(t) \end{pmatrix} \tag{2}$$

describes the rotation of the IMU around the x-, y- and z-axis. A common problem with gyroscopes is drift, or rather a slowly varying bias, which causes a growing error in the calculated orientation. However, in the hovering scenario, the average orientation should be constant, so we can suppress the slowly varying bias with a high-pass filter.

To calculate the position of the IMU, we use the calculated orientation to remove the rotation from the acceleration data. Then, we can calculate the average acceleration in the vertical direction and subtract it from the z-component of the data to compensate for the gravity. After integrating the acceleration data twice, we receive the IMU position

$$\mathbf{p}_\mathrm{IMU}(t) = \begin{pmatrix} x_\mathrm{IMU}(t) \\ y_\mathrm{IMU} t \\ z_\mathrm{IMU}(t) \end{pmatrix} . \tag{3}$$

Again, we filter the acceleration data and the resulting position $\mathbf{p}_\mathrm{IMU}(t)$ in each component with a high-pass filter to ensure that the calculated vibration has a constant center [8][9].

III. Motion Analysis and Compensation Strategies

In this section, we describe the effects of motion in the different degrees of freedom and propose compensation strategies. For each compensation algorithm, we also describe the computational complexity.

A. Rotation around x- or y-Axis

If the radar system rotates $\mathrm{d}\beta$ degree around the y-axis between two measurements, this will result in a shift in the Range-Azimuth (RA) map. Consequently, a peak corresponding to a reflection from an angle Φ, which was located at the spatial frequency

$$k = \frac{2\pi \mathrm{d}x \sin(\Phi)}{\lambda} \tag{4}$$

in the RA map, is now located at

$$k' = \frac{2\pi \mathrm{d}x \sin(\Phi + \mathrm{d}\beta)}{\lambda}, \tag{5}$$

where $\mathrm{d}x$ is the horizontal distance of the antennas in the virtual array. This means that after the rotation, the target may be located in a different voxel, depending on the strength of the rotation and the resolution of the RA map. For a single measurement, this shift is not a problem. However, if the application involves the detection of humans, the shift can result in blurred peaks in the detector output. Furthermore, the phase extracted from the detected voxel will contain jumps due to the fact that the human target was not present in this voxel in every time step. A rotation around the x-axis has a similar effect on the elevation of targets. For the sake of simplicity, we will only describe the compensation for the rotation around the y-axis, but the compensation for a rotation around the x-axis can be deduced directly from it [6][10][11].

A possible counter-strategy would be to use shorter integration intervals for the detector, so that the considered interval contains only small changes of the rotation angle β. This approach would increase the computational effort while it would reduce the signal-to-noise ratio (SNR) of the detector. Moreover, there could still be fast changes of the orientation for which the interval length is too large to prevent all voxel jumps. To solve this problem without limiting the integration interval of the detector, we propose an approach using the gyroscope data measured by the IMU.

To clarify the effect of the rotation, we can analyze the error of the location in the azimuth map resulting from the rotation. The location of a target in the azimuth map at an angle Φ

after the rotation is compared with the original location of the target using

$$\begin{aligned}\epsilon_{\text{rot}} &= \left|\frac{1}{2}\left(\sin(\Phi) - \sin(\Phi + \mathrm{d}\beta)\right)\right| \\ &= \left|\frac{1}{2}\left(\sin(\Phi) - \left(\sin(\Phi)\cos(\mathrm{d}\beta) + \cos(\Phi)\sin(\mathrm{d}\beta)\right)\right)\right| \\ &= \left|\frac{1}{2}\left(\sin(\Phi)\left(1 - \cos(\mathrm{d}\beta)\right) - \cos(\Phi)\sin(\mathrm{d}\beta)\right)\right| \quad . \end{aligned} \tag{6}$$

For the sake of simplicity, we set $\mathrm{d}x = \frac{\lambda}{2}$. If we assume the maximal rotation between two measurements is 20°, we can use $(1-\cos(\mathrm{d}\beta)) < 0.06$ to simplify equation (6). This results in

$$\epsilon_{\text{rot}} \approx \left|-\frac{1}{2}\cos(\Phi)\sin(\mathrm{d}\beta)\right|, \tag{7}$$

showing that the error is high for small angles Φ and low for large angles. Regarding the application, this behavior is quite unsuitable while the inverse properties, more precisely low errors for small angles Φ and high errors for large angles, would be suitable for the application. The error with inverse properties can be described with

$$\epsilon_{\text{rot}} \approx \left|\frac{1}{2}\left(1 - \cos(\Phi)\right)\sin(\mathrm{d}\beta)\right|. \tag{8}$$

If we reverse the neglect of the term $\sin(\Phi)\left(1 - \cos(\mathrm{d}\beta)\right)$, it will follow

$$\begin{aligned}\epsilon_{\text{rot}} &= \left|\frac{1}{2}\left(\sin(\Phi)\left(1 - \cos(\mathrm{d}\beta)\right) + \sin(\mathrm{d}\beta)\left(1 - \cos(\Phi)\right)\right)\right| \\ &= \Big|\frac{1}{2}(\sin(\Phi) - \sin(\Phi)\cos(\mathrm{d}\beta) \\ &\qquad - \cos(\Phi)\sin(\mathrm{d}\beta) + \sin(\mathrm{d}\beta))\Big| \\ &= \left|\frac{1}{2}\left(\sin(\Phi) - \left(\sin(\Phi + \mathrm{d}\beta) - \sin(\mathrm{d}\beta)\right)\right)\right| \quad . \end{aligned} \tag{9}$$

This means that we can compensate the rotation for smaller angles Φ by shifting the peak in the azimuth domain with

$$\mathrm{d}k = -\frac{2\pi \mathrm{d}x \sin(\mathrm{d}\beta)}{\lambda} \quad . \tag{10}$$

The azimuth map is calculated by taking the Fourier transform over the signals of the different antennas in the spatial domain. A shift by $\mathrm{d}k$ in the azimuth domain can be represented as the multiplication

$$G'(r, x) = G(r, x) \cdot \exp(\mathrm{i} \cdot 2\pi \cdot \mathrm{d}k \cdot x) \tag{11}$$

in the spatial domain, where i is the imaginary unit with $\mathrm{i} = \sqrt{-1}$, x is the x-component of the antenna position in the virtual array, and $G(r, x)$ is the signal in range r and antenna position x after applying the Fourier transform in the range domain. The error with and without compensation is shown in figure 1.

Due to the fact that the true rotation angle $\beta(t)$ at time t is unknown, we need to use the the rotation angle calculated from the IMU data $\beta_{\text{IMU}}(t)$ to compensate the rotation. If the

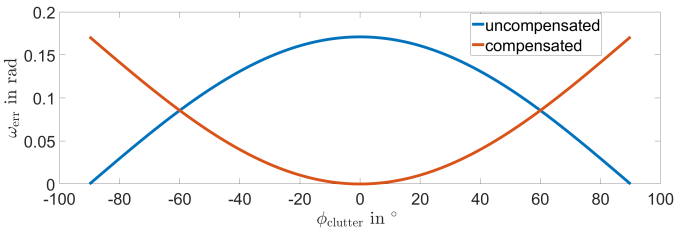

Fig. 1. Depiction of the error induced by the rotation around the y-axis with and without compensation.

IMU data contains a measurement error $e = \mathrm{d}\beta_{\text{IMU}} - \mathrm{d}\beta$, the effect of this measurement error can be calculated with

$$\begin{aligned}\epsilon_{\text{IMU}} &= \Big|\frac{1}{2}(\sin(\Phi) - (\sin(\Phi + \mathrm{d}\beta) - \sin(\mathrm{d}\beta))) \\ &\qquad -\frac{1}{2}(\sin(\Phi) - (\sin(\Phi + \mathrm{d}\beta) - \sin(\mathrm{d}\beta_{\text{IMU}})))\Big| \\ &= \left|\frac{1}{2}(\sin(\mathrm{d}\beta) - \sin(\mathrm{d}\beta + e)))\right| \\ &= \left|\frac{1}{2}(\sin(\mathrm{d}\beta) - \sin(\mathrm{d}\beta)\cos(e) - \cos(\mathrm{d}\beta)\sin(e))\right| \\ &= \left|\frac{1}{2}(\sin(\mathrm{d}\beta)(1 - \cos(e)) - \cos(\mathrm{d}\beta)\sin(e))\right|. \end{aligned} \tag{12}$$

Assuming the measurement error e is way smaller than $\mathrm{d}\beta$, $(1 - \cos(e)) \approx 0$ can be used to simplify equation (12) to

$$\epsilon_{\text{IMU}} \approx \left|-\frac{1}{2}\cos(\mathrm{d}\beta)\sin(e)\right|. \tag{13}$$

Using the linearity of the sine-function around zero and the assumption that the rotation angles are smaller 20°, this can be approximated to

$$\epsilon_{\text{IMU}} \approx \frac{1}{2}e \ . \tag{14}$$

This means that the measurement error e adds a linear term, depending only on the measurement error e, to the location error. Consequently, the location error after compensating the rotation with the IMU data can be approximated with

$$\epsilon \approx \left|\frac{1}{2}((1 - \cos(\Phi))\sin(\mathrm{d}\beta) - e)\right| \tag{15}$$

After compensation, the peak corresponding to an object should be in the same azimuth bin of the RA map as the peak of the object without rotation would be. If the FFT in the azimuth direction uses $n_\Phi = 16$ points, the maximal error

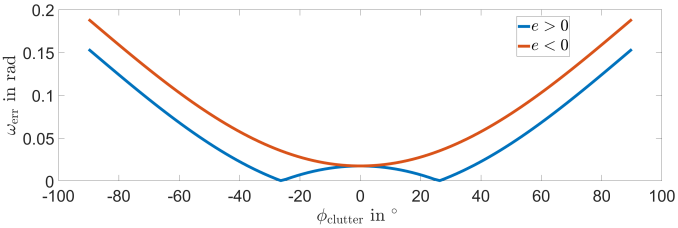

Fig. 2. Depiction of the error resulting from the inaccurate rotation angle calculated from the IMU data for a positive (blue) and negative (red) error of the estimated rotation angle

allowed after the compensation is $\epsilon_{\max} = 1/n_\Phi = 0.0625$. For a rotation of 20° and a relative error of 10 % the resulting error depending on the angle Φ is depicted in figure 2. It is easy to see that for all angles Φ smaller than $\pm 40°$ this restriction is fulfilled. If the magnitude of $\mathrm{d}\beta_{\mathrm{IMU}}$ is larger than $\mathrm{d}\beta$, the restriction will be fulfilled even for all angles Φ smaller than $\pm 60°$. As shown in equation (11), the compensation only involves an element wise multiplication with a complex factor. Therefore, the computational complexity of the compensation for one time step t is only depending on the size of $G(r, m_{\mathrm{x}}, m_{\mathrm{y}}, t)$ or more precisely the number of antennas in the virtual array and the number of range bins.

B. Rotation around z-Axis

The effect of a rotation around the z-axis on the radar signal depends on the azimuth and elevation angle of the object reflecting the signal. For objects in the center of the azimuth-elevation (AE) map, a rotation around the z-axis has barely an effect because they are also in the center of the rotation. In reference to the considered application, this means that the rotation has almost no effect on the reflection from the ground. For objects with larger azimuth or elevation angles, the rotation results in a displacement in the AE map. There are already some investigations and compensations techniques regarding rotations of radar systems [10][12][13], but they are not really applicable for a MIMO radar mounted underneath a UAV.

Since the rotation around the z-axis results in a rotated virtual array, we need to find the signals that would have been received by the antennas at the original positions without rotation. The signal $G(r, m_{\mathrm{x}}, m_{\mathrm{y}}, t)$ is received by the antenna element $(m_{\mathrm{x}}, m_{\mathrm{y}})$. We can describe its position with the vector

$$\mathbf{b}(m_{\mathrm{x}}, m_{\mathrm{y}}, t) = \begin{pmatrix} x(m_{\mathrm{x}}, t) & y(m_{\mathrm{y}}, t) \end{pmatrix}^{\mathrm{T}} . \tag{16}$$

With $\gamma_{\mathrm{IMU}}(t)$ as the rotation angle around the z-axis calculated from the IMU data, we can calculate a rotated version of the virtual antenna position

$$\begin{aligned} \mathbf{b}(m_{\mathrm{x}}, m_{\mathrm{y}}, t)' &= \begin{pmatrix} x(m_{\mathrm{x}}, t)' \\ y(m_{\mathrm{y}}, t)' \end{pmatrix} \\ &= \begin{pmatrix} x(m_{\mathrm{x}}, t) \\ y(m_{\mathrm{y}}, t) \end{pmatrix} \cdot \begin{pmatrix} \cos(-\gamma_{\mathrm{IMU}}(t)) & -\sin(-\gamma_{\mathrm{IMU}}(t)) \\ \sin(-\gamma_{\mathrm{IMU}}(t)) & \cos(-\gamma_{\mathrm{IMU}}(t)) \end{pmatrix} . \end{aligned} \tag{17}$$

The positions $\mathbf{b}(k_{\mathrm{x}}, k_{\mathrm{y}}, t)'$ can be used to interpolate the expected signals at the antenna positions without rotation. As interpolation method we use the bilinear interpolation which calculates the interpolation value by looking at a 2×2 environment of the considered point. For each antenna element $(m_{\mathrm{x}}, m_{\mathrm{y}})$, we first need to find the elements belonging to the 2×2 environment. Therefore, every possible x-value of the non-rotated antenna positions $x(i_{\mathrm{x}}, t)$ with $i_{\mathrm{x}} = 1, ..., M_{\mathrm{x}}$ is compared with the x-value of the currently considered rotated antenna position $x(m_{\mathrm{x}}, t)'$. The values with the smallest absolute difference are then defined as x_1 and x_2. Similarly, we define y_1 and y_2 by comparing the y-values. The four antenna positions $\{(x_1, y_1), (x_1, y_2), (x_2, y_1), (x_2, y_2)\}$ build a rectangle. With the weighted mean

$$\begin{aligned} G(r, m_{\mathrm{x}}, m_{\mathrm{y}}, t)' = {} & w_{11} \cdot G(r, x_1, y_1, t) + w_{12} \cdot G(r, x_1, y_2, t) \\ & + w_{21} \cdot G(r, x_2, y_1, t) + w_{22} \cdot G(r, x_2, y_2, t) \end{aligned} \tag{18}$$

and the coefficients

$$\begin{pmatrix} w_{11} \\ w_{12} \\ w_{21} \\ w_{22} \end{pmatrix} = \begin{pmatrix} 1 & 1 & 1 & 1 \\ x_1 & x_1 & x_2 & x_2 \\ y_1 & y_2 & y_1 & y_2 \\ x_1 y_1 & x_1 y_2 & x_2 y_1 & x_2 y_2 \end{pmatrix}^{-1} \begin{pmatrix} 1 \\ x' \\ y' \\ x' y' \end{pmatrix} \tag{19}$$

the rotated signal can be calculated [14]. Here x' and y' describe the rotated antenna position of the currently interpolated element. If this is done for all antenna elements $(m_{\mathrm{x}}, m_{\mathrm{y}})$ and range indices r at one time step t, the signals can be used to compute the approximate non-rotated voxels at this time step.

The accuracy of the compensation depends on the accuracy of the rotation angle $\gamma_{\mathrm{IMU}}(t)$ measured by the IMU. Since rotations around the z-axis have barely an effect on signals reflected from small azimuth and elevation angles, and since the resolution in the azimuth-elevation domain is quite low for angles larger than 15°, only rotations larger than 20° have a significant effect on the measured data while rotations smaller than 20° are barely noticeable. Therefore, errors of the estimated rotation angle $\gamma_{\mathrm{IMU}}(t)$ have also no effect on the compensated data as long as they are smaller than 20°.

Compared to the compensation of the rotation around the x- or y-axis, the computational complexity of compensating for rotations around the z-axis is much higher. First, the points in the virtual array have to be rotated using the matrix multiplication described in equation (17). Then, for each rotated point the nearest points in the virtual array without rotation have to be located. For an equidistant virtual array with the distance d_{ant} between the antenna elements, this can be done by scaling the rotated points with $\frac{1}{d_{\mathrm{ant}}}$ and using floor and ceil operators. Afterwards, the weights can be calculated using the matrix multiplication in equation (19). The points x_1, x_2, y_1 and y_2 as well as the weights differ for the different virtual antenna elements but are the same for all corresponding range bins. This means that if the weights have been calculated for all rotated virtual antenna elements, we can use them to calculate the compensated representation with the weighted mean (18) for all range bins. Using a numerical analysis, we have found that the compensation of the rotation around the z-axis takes about eight times longer than the compensation of the rotation around the x- and y-axis. The overall computation time can be reduced by executing the compensation only for rotation angles $\gamma_{\mathrm{IMU}}(t)$ larger than some threshold angle.

C. Vibration in z-Direction

For a ground-looking radar, the vibrations in z-direction have the most significant effect. The vertical vibrations change the radial distance to the targets on the ground. Therefore, the vertical vibrations disturb the phase of the measured signals massively. There are already several approaches to reduce their influence [15]. Most of them are using reflections from static objects to estimate the vertical motion of the UAV. In [1][2], they use additional radar systems or other distance

measurement systems to estimate the vertical vibration. The problem with these approaches is the additional weight and computational effort which both put a strain on the restricted resources on the UAV. Another approach is to rely on the fact that there will always be a signal belonging to static clutter from which the vertical motion of the radar can be extracted [3]. This approach will be problematic if the dynamic target lies in the focus of the radar and the UAV is not flying very high. In this case, the signal extracted from the dynamic target would be used to estimate the vertical motion of the UAV. Similar to the approach in [3], we propose to only use one radar for the estimation of the vertical motion and the extraction of the motion of the dynamic targets. But we add an algorithm which ensures that the vertical motion is extracted from a static target.

The effect of the motion of the radar system onto the phase $\phi_{\text{stat}}(t)$ of a signal, reflected from a static target at an azimuth angle Φ_{stat} and an elevation angle Θ_{stat}, can be seen as an orthogonal projection onto the steering vector to the target. A two dimensional depiction of his projection is shown in figure 3. Here

$$\mathbf{e} = \begin{pmatrix} \sin(\Phi) \\ \sin(\Theta) \\ \cos(\Phi)\cos(\Theta) \end{pmatrix} \tag{20}$$

is the steering vector in target direction, $\mathbf{p}(t)$ is the current position of the moving radar system and $u(t)$ is the resulting change of the radial distance to the target. This can also be described as

$$\begin{aligned} u(t) =& \frac{\mathbf{p}(t)^{\mathrm{T}} \cdot \mathbf{e}}{\|\mathbf{e}\|} \\ =& \frac{1}{\|\mathbf{e}\|} \begin{pmatrix} x(t) \\ y(t) \\ z(t) \end{pmatrix}^{\mathrm{T}} \cdot \begin{pmatrix} \sin(\Phi_{\text{stat}}) \\ \sin(\Theta_{\text{stat}}) \\ \cos(\Phi_{\text{stat}})\cos(\Theta_{\text{stat}}) \end{pmatrix}. \end{aligned} \tag{21}$$

The norm $\|\mathbf{e}\|$ is approximately 1. Therefore, equation (21) can be simplified to

$$\begin{aligned} u(t) \approx& \cos(\Phi_{\text{stat}})\cos(\Theta_{\text{stat}})z(t) + \\ & \sin(\Phi_{\text{stat}})x(t) + \sin(\Theta_{\text{stat}})y(t) \ . \end{aligned} \tag{22}$$

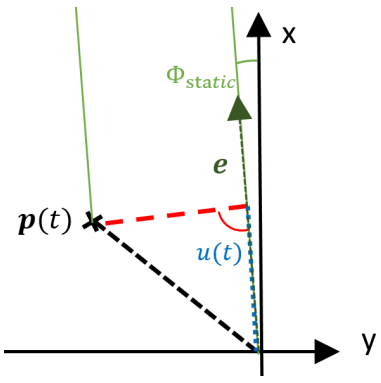

Fig. 3. Depiction of the orthogonal projection from the radar position $\mathbf{p}(t)$ onto the steering vector $\mathbf{e}$

For small azimuth and elevation angles the x- and y-component can be neglected. Hence, the equation can be approximated to

$$u(t) \approx \cos(\Phi_{\text{stat}})\cos(\Theta_{\text{stat}})z(t). \tag{23}$$

This means that if we want to estimate the vertical vibration of the radar system, we can evaluate the phase reflected from static targets with small azimuth and elevation angles. In most cases, the strongest reflection in the central area of the azimuth elevation domain should correspond to the reflection from the ground. However, there is a possibility that a person lies directly in the focus of the radar. Therefore, we propose to determine the voxel containing a reflection from the ground by evaluating all reflections with azimuth and elevation angles up to $\pm 10°$.

To find signals reflected from objects with high RCS, we use the following detector

$$D_{\text{mag}}(r,\Phi,\Theta) = \sum_{t=0}^{T_{\text{floor}}} \left| f(r,\Phi,\Theta,t) \right| . \tag{24}$$

which evaluates the magnitude of the reflected signals. Here T_{floor} is the length of the interval which is used to detect the floor. After applying the magnitude detector, we extract the signals from all voxels that have a detection value greater than

$$D_{\text{min}} = \psi \cdot \max(|D_{\text{mag}}(r,\Phi,\Theta)|), \tag{25}$$

where $\psi \in \mathbb{R}$ is a constant between 0 and 1. The slowtime signals $s_k(t)$ with $k = 1, ..., K$ extracted from the detected voxels are then evaluated to find a reflection from a static object. To ensure that the detection belongs to a static object, we want to find the signal with maximum similarity to the vibrations in z-direction $z_{\text{IMU}}(t)$ calculated from the IMU data, while the signal should not contain strong frequency components that do not belong to the vertical motion.

Let

$$z_k(t) = \phi_k(t) \cdot \frac{\lambda}{4\pi} \frac{1}{\cos(\Theta_k)\cos(\Phi_k)} \tag{26}$$

be the motion in z-direction estimated from the k^{th} detection, where Φ_k and Θ_k are the azimuth and elevation angles of the k^{th} detection. Let further $Z_k(f)$ and $Z_{\text{IMU}}(f)$ be the FFT of $z_k(t)$ and $z_{\text{IMU}}(t)$. By taking all frequencies belonging to strong values in $Z_{\text{IMU}}(f)$, we can form the set Ω_{static}. We can then define $\mathbf{w}_k$ and $\mathbf{w}_{\text{IMU}}$ as the vectors built of all elements of $Z_k(f)$ and $Z_{\text{IMU}}(f)$, respectively, which are involved in Ω_{static}. Furthermore, we define an application dependent set Ω_{dyn} involving the frequencies which could be expected to be resulting from a target motion. For the application considered in this paper, the set contains all possible respiration frequencies.Therefore, the vector $\mathbf{v}_k$ is built of all elements of $Z_k(f)$ which are involved in Ω_{dyn}. With

$$\hat{k} = \underset{k\in[1,\ldots,K]}{\arg\min} \ \|\mathbf{w}_k - \mathbf{w}_{\text{IMU}}\|_2 + \mu \|\mathbf{v}_k\|_2 \tag{27}$$

we estimate the index $\hat{k}$ of the signal which has the highest probability to belong to a static clutter. Here μ is a constant with a value between 0 and 1 that balances the two optimization terms.

To enable the use of the phase $\phi_{\hat{k}}(t)$, selected with the optimal index $\hat{k}$ for the motion compensation, we need to project it onto the z-axis with

$$\phi_{\text{comp}}(t) = \frac{\phi_{\hat{k}}(t)}{\cos(\Phi_{\hat{k}})\cos(\Theta_{\hat{k}})}. \tag{28}$$

Afterwards, $\phi_{\text{comp}}(t)$ can be used to compensate the vibration in z-direction in each voxel with

$$\begin{aligned} f_{\text{comp}}(r,\Phi,\Theta,t) =& f(r,\Phi,\Theta,t) \\ &\cdot \exp(-\mathrm{i}\cdot\phi_{\text{comp}}(t)\cos(\Phi)\cos(\Theta)). \end{aligned} \tag{29}$$

In equation (29), the term $\cos(\Phi)\cos(\Theta)$ ensures that the vibration in z-direction is projected onto the direction of the currently considered voxel. In the resulting signal $f_{\text{comp}}(r,\Phi,\Theta,t)$ the motion of dynamic targets should be the strongest component. In a Doppler detector

$$D_{\text{doppler}}(r,\Phi,\Theta) = \sum_{f\in\Psi} |F(r,\Phi,\Theta,f)|, \tag{30}$$

where Ψ is a set of frequencies at which the target motion is expected, only the dynamic targets should have high values [16]. Moreover, the signals extracted from some detected human should only contain the motion of the target itself and should not be disturbed by the vibration of the radar in z-direction.

For the calculation of the computational complexity, we have to distinguish between the localization of the voxel containing the reflection of the floor and the compensation of the vertical motion. The detection of the floor is performed every T_{floor} seconds and an interval of T_{floor} seconds is analyzed. Therefore, the complexity for the detection itself scales with T_{floor}, but considering a longer duration, T_{floor} affects the computational complexity only as a constant. Moreover, the total number of voxels considered also depends on the azimuth and elevation resolution, since the resolution influences how many voxels are considered as floor voxel. The compensation of the vibrations in z-direction is executed in each time step and involves an element wise multiplication of all voxels with the complex compensation term. The computational complexity scales with the number of range, azimuth and elevation bins.

D. Vibration in x- or y-Direction

As described in Section III-C, the effect of the radar motion on the phase signal depends on the target elevation and azimuth angle. More specifically, the part of the radar vibration that should be present in the phase signal can be calculated by orthogonal projection onto the steering vector $\mathbf{e}$ pointing to the target. While the effect of the vibration in z-direction is most significant for small angles Φ and Θ, the influence of the vibrations in x- and y-direction is increasing with increasing values of Φ and Θ. For the considered application, we only look at azimuth and elevation angles smaller $\pm 40°$. Therefore, the effect of the horizontal motions is much smaller than the effect of the vertical vibrations. Hence, the human targets can be detected although there are still horizontal motions affecting the signals. However, in order to evaluate the vital signs, these movements have to be compensated as well.

All following computations are performed on the signals for which the vertical motion has been compensated, otherwise the horizontal motion can not be separated from the vertical motion. Again, we estimate the radar motion by evaluating the reflection from static objects. Therefore, the magnitude detector from equation (24) is used. Since the effect of horizontal motion increases with increasing azimuth and elevation angles, only angles larger $\pm 15°$ are evaluated. We also need to distinguish between the vibrations in x- and y- direction. For the estimation of the motion in x-direction, we consider only the voxels with elevation angle equal to zero, while for the estimation of the motion in y-direction, we consider only the voxels with azimuth angle equal to zero. Additionally, we mask the detector output in the area where the target was located.

To find static objects from which the motion in x-direction can be estimated, we evaluate all phase signals $\phi_k(t)$ with $k = 1, ..., K_{\text{x}}$, for which the detector output is greater than a threshold calculated with equation (25). Using the orthogonal projection from equation (21), the considered phase signals can be be interpreted as motion in x-direction with

$$x_k(t) = \phi_k(t)\cdot\frac{\lambda}{4\pi}\frac{1}{\sin(\Phi_k)}. \tag{31}$$

Instead of the vertical motion, the motion in x-direction $x_{\text{IMU}}(t)$ calculated from the IMU data is used for comparison with the phase signals. Then, the optimization method (27) can be used in a similar way as in the previous section to determine the index $\hat{k}$ corresponding to a voxel containing the reflection of a static object. Afterwards, the compensation signal can be calculated with

$$\phi_{\text{x}}(t) = \frac{\phi_{\hat{k}}(t)}{\sin(\Phi_{\hat{k}})}. \tag{32}$$

The vibration in y-direction can be calculated in a similar fashion using the detector output for azimuth angles equal zero, the y-component of the IMU motion, and the orthogonal projection with $\sin(\Theta_k)$ instead of $\sin(\Phi_k)$. The estimated signals are then used to compensate the contained horizontal motion in the signal extracted from the human target $s_{\text{dyn}}(t)$ with

$$\begin{aligned} \tilde{s}_{\text{dyn}}(t) =& s_{\text{dyn}}(t) \\ &\cdot \exp\left(-\mathrm{i}(\phi_{\text{x}}(t)\sin(\Phi_{\text{dyn}}) + \phi_{\text{y}}(t)\sin(\Theta_{\text{dyn}}))\right). \end{aligned} \tag{33}$$

The computational complexity of the static target determination is comparable to the static target determination for the vertical motion. However, the compensation of the horizontal movements is executed on the extracted slowtime signal. Therefore, the computational complexity is only depending on the length of the extracted signal and the overall computational effort for the compensation of the vibrations in x- and y-direction is negligible compared to the other compensations presented in this paper.

IV. Results

A. Measurement Setup

To analyze the algorithmic solutions, we want to consider each degree of freedom independently. Since it is difficult to

ensure that a UAV has a vibration or a rotation in only one direction, we use a setup that is as close as possible to the application of a UAV searching for humans. Therefore, we mount the radar system together with the IMU on a tripod so that the radar system points to a wall. In this case, the direct line from the radar system to the wall corresponds to the z-axis in the original scenario while the vertical axis in the measurement setup is the y-axis of the original scenario. The axis parallel to the wall and the floor crossing the radar system represents the x-axis of the original scenario. Since in the original application we search for a person lying on the ground, we use a person standing directly in front of the wall in the measurement setup. The position of the person along the x-axis or the azimuth angle as seen by the radar, can be varied. To show the capabilities of the proposed algorithms, we use a measurement time of 30 seconds and do not process the data in separated intervals.

As radar systems, we used two different 60 GHz radars. For the measurements in which we rotate the radar system around the z-axis, we used a TI IWR 6843AOP evaluation board [17] because it has a 4×4-topology[2] and therefore a symmetrical resolution in azimuth and elevation. For all other measurements, we used a TI IWR 6843 ISK evaluation board [18] with an 8×2 topology because it has the higher resolution in the azimuth domain. We configured both radar systems with a chirp repetition rate of 500 Hz and a bandwidth of 1 GHz. As IMU, we used a BNO055 [19], which is a low cost MEMS-based IMU containing a gyroscope, an accelerometer and a magnetometer. To validate our measurements, a reference system, measuring the breathing motion of the test person, was used [20].

B. Vibration in z-Direction

For the evaluation of the compensation of vertical vibrations, the person was standing at $10°$ azimuth and the radar system was moved in a sinusoidal fashion with a frequency of about 2 Hz and a magnitude of 3 cm. The left image in figure 4 shows the range-azimuth (RA) map of the Doppler detector without using the compensation. As the radar is moving, every object in the scene, including the wall, is moving relative to the radar. Since the wall has the largest RCS, it will generate the highest magnitude in the Doppler detector. Therefore, it is impossible to detect the person in the scene. The right image in figure 4 shows the output of the Doppler detector after compensating the vertical motion of the radar. Here, the wall does not generate a peak because the motion of the radar is compensated. Hence, the strongest value in the Doppler detector corresponds to the reflection from the person. If we extract the signal from this voxel over time and calculate the unwrapped phase signal, we can analyze the breathing motion of the person. In figure 5, the unwrapped phase signal from the voxel with the person is shown together with the unwrapped phase signal from the same voxel without compensation and the breathing motion measured by the reference system. Since the compensated signal is comparable to the breathing motion measured by the reference system, the accuracy of the compensation method is proven.

The comparable approaches [1], [2] and [3] all lack a distinction between static and dynamic targets when estimating the vertical motion of the radar system. To visualize the effect of the proposed floor voxel determination, we positioned the person in the focus of the radar at $0°$ azimuth. Then, we use the method described in III-C and the equation (27) to find

[2]To get the 4×4-topology 4 of the 16 channels need to be zero-padded, because the radar system only has 3 transmitters and 4 receivers.

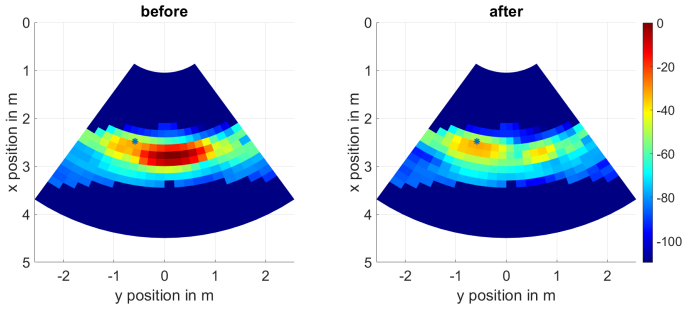

Fig. 4. Depiction of the RA map before and after the compensation of the vibration in z-direction. The blue markers show the position of the person at $10°$ azimuth.

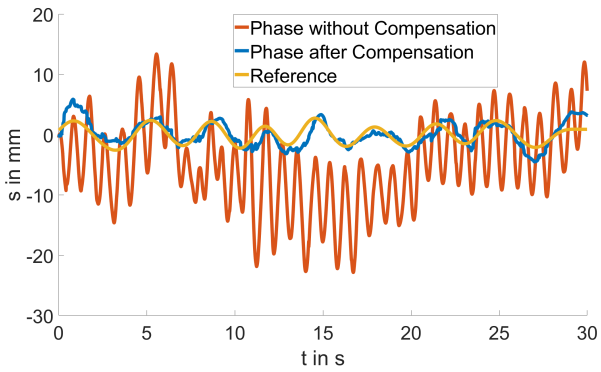

Fig. 5. Depiction of the phase signal from a person before and after the compensation of the vibration in z-direction together with the breathing motion measured by the reference system.

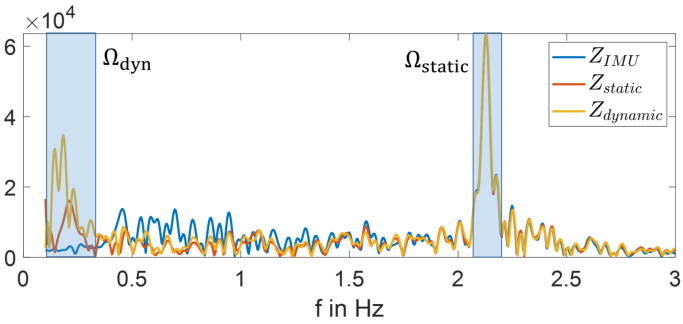

Fig. 6. Depiction of the spectrum corresponding to the reflection of a static target (red) and a dynamic target (yellow) together with the spectrum of the vibration in z-direction calculated from the IMU data. The light blue boxes mark the frequency area of the motion of the radar Ω_{static} and the breathing motion of humans Ω_{dyn}.

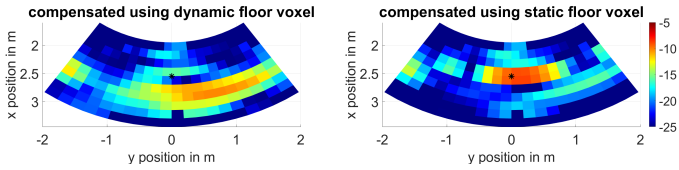

Fig. 7. Depiction of the RA domain after the compensation of the vibration in z-direction with a signal extracted from the central voxel as in [3] (left) and a signal extracted from a static target (right). The black markers show the true position of the person at $0°$ azimuth.

the strongest reflection from a static target. In this example we set the balancing term to $\mu = 0.8$. The figure 6 shows the spectrum of the selected signal, extracted from a voxel with $6°$ azimuth, together with the spectrum of the signal generated by the dynamic target at $0°$ and the spectrum of the motion in z-direction calculated from the IMU data. It is easy to see that both radar signals consist of the true motion in z-direction at 2.1 Hz but the spectrum of the dynamic target has the higher energy in the frequency range Ω_{dyn} which contains the possible breathing rates of humans. This shows that the signal extracted from $0°$ azimuth belongs to a human while the selected signal most likely corresponds to a reflection from the wall. Therefore, it can be used to compensate the vibration in z-direction. Figure 7 shows the output of the Doppler detector after compensating the vertical motion with the signal from the dynamic target and after compensating the vertical motion with the signal from the static target. For the compensation with the signal extracted from the dynamic target, which probably would have been extracted without the determination of the ground voxel, there is no strong peak at the true position of the person. If the signal extracted from the static target, selected with the proposed algorithm, is used for the compensation, the motion will be compensated correctly and the target will be detected at its true position.

C. Vibration in x- or y-Direction

To evaluate the compensation of the horizontal vibrations, the radar system is moved along the x-axis in a sinusoidal motion with an amplitude of 4 cm and a frequency of about 2 Hz. The person is standing at $15°$ azimuth with contact to the wall. In a first step, we remove any vibration in z-direction with the algorithm described in Section III-C and detect the person with a Doppler detector.

After extracting the slowtime signal from the voxel with the person, we can use the algorithm described in Section III-D to remove the vibrations in x- and y-direction. Again, the balancing term was set to $\mu = 0.8$ and the motion in x-direction was extracted from a static target at $-23°$. Figure 8 shows the result of this compensation. In the signal that was compensated only in z-direction, a high frequency vibration is present, while in the signal that was also compensated in x-direction, the respiratory motion can be identified easily. For comparison, we have also plotted the respiratory motion measured by the reference system .

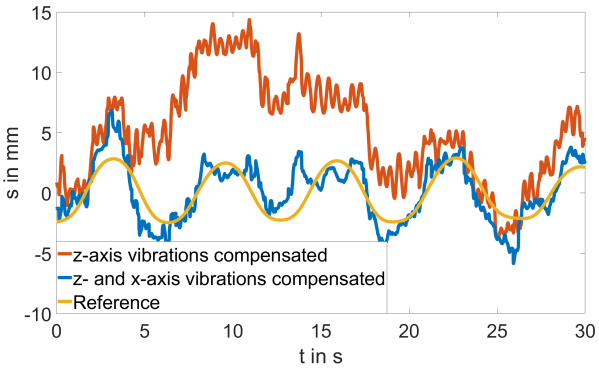

Fig. 8. Depiction of the phase signal from a person before and after the compensation of the vibration in x-direction together with the breathing motion measured by the reference system.

D. Rotation around x- or y-Axis

In order to demonstrate the capabilities of the rotation compensation around the x- or y-axis, the radar system was continuously rotated around the y-axis with a magnitude of $20°$. For this measurement, the person was standing at $15°$ azimuth with contact to the wall. The upper left plot of Figure 9 shows the RA map of the Doppler detector for a measurement that includes vibrations in z-directions and rotations around the y-axis. Resulting from the rotation, the energy of the main reflection from the wall is distributed over all azimuth angles between $-30°$ and $30°$. If only the compensation algorithm for the vibration in z-direction is used, the resulting representation can not be evaluated because the reflection from the wall can not be extracted correctly. The corresponding detector output is shown in the upper right image. If the rotation around the y-axis is compensated, for which the detector output is shown in the lower left image, we can detect a strong reflection in the center of the range-azimuth plane belonging to the reflection of the wall. If we then use the vibration compensation in z-direction, the Doppler detector will look like the lower right image of Figure 9 and finally the person can be detected at $15°$ azimuth.

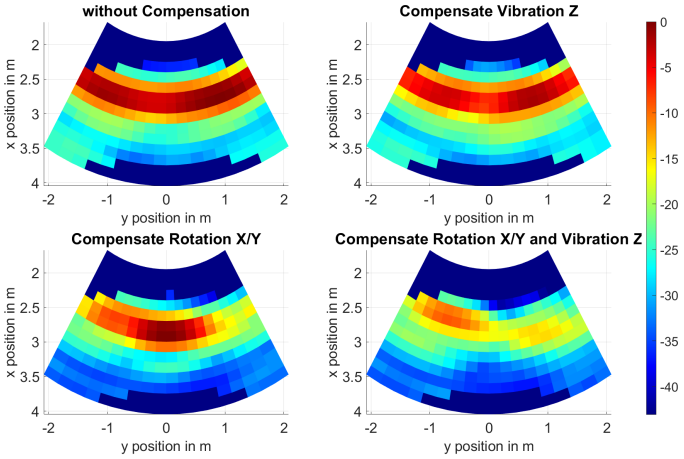

Fig. 9. Depiction of the compensation of the rotation around the y-axis in combination with the compensation of the vibrations in z-direction.

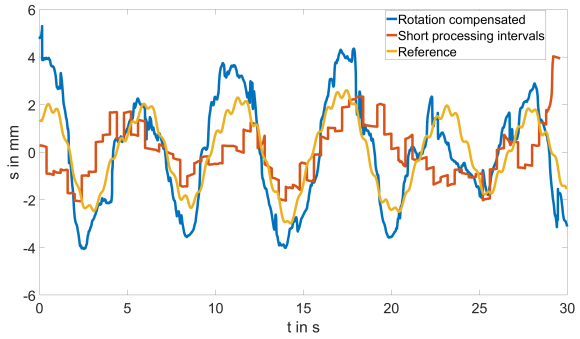

Fig. 10. Depiction of the phase signal from a person extracted using rotation compensation (blue) and short processing intervals (red) together with the breathing motion measured by the reference system (yellow).

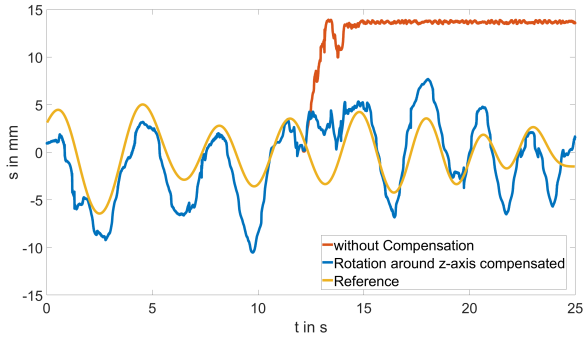

Fig. 12. Depiction of the unwrapped phase signal with and without the compensation of the rotation around the z-axis together with the breathing motion measured by the reference system.

An alternative approach to compensate for the rotation would be to use shorter processing intervals and tracking to follow the target as the radar system rotates. Figure 10 shows the phase extracted using rotation compensation together with a signal extracted using short processing intervals and the breathing motion measured by the vital sign reference system. It is clear to see, that the signal extracted using rotating compensation is more accurate. The signal extracted using short processing intervals suffers from many jumps generated by the concatenation of the intervals, while the signal extracted using rotation compensation could be extracted continuously from one voxel. In this case, an interval length of 0.5 seconds was used. For shorter or longer intervals the quality of the extracted signal was even worse. For applications such as the evaluation of the breathing rate, the long coherent measurements provided by the rotation compensation improve the signal quality and thus the accuracy of the measured vital signs.

E. Rotation around z-Axis

To simulate a rotation of the UAV around the z-axis, we performed a measurement with a duration of 25 seconds. After 12 seconds, the radar system was rotated by $80°$ around the axis pointing towards the wall. The azimuth-elevation (AE) map of the Doppler detector without any compensation is shown in the left image of Figure 11. Resulting from the rotation, the peak corresponding to a person at $20°$ azimuth is shifted or rather spread over the AE map, because for the first 12 seconds of the measurement the person was located at $-20°$ azimuth and $-10°$ elevation as seen from the radar while for the remaining 13 seconds of the measurement the person was located at $-5°$ azimuth and $20°$ elevation. The right image shows the AE map of the Doppler detector after the compensation of the rotation around the z-axis. Due to the compensation, the target remains at the same location throughout the measurement, resulting in a focused peak.

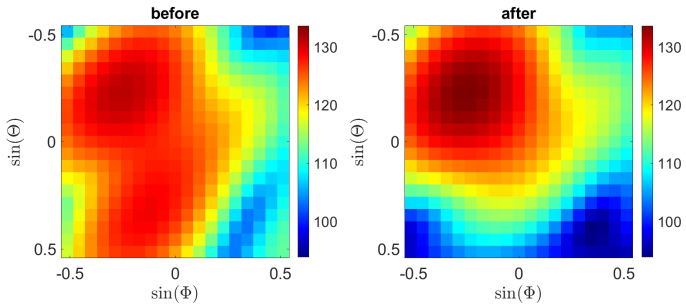

Fig. 11. Depiction of the RA map before and after the compensation of the rotation around the z-axis.

Since the maximum of the Doppler detector should correspond to the voxel with the person, we can use it to extract the slowtime signals and calculate the unwrapped phase signal. Figure 12 shows these unwrapped phase signals for the measurement with and without compensation. It can be seen, that without the compensation the respiration signal can only be evaluated for the first 12 seconds. After 12 seconds, the radar system has been rotated, which means that the signal does not contain any reflections from the person. However, the phase signal calculated from the compensated measurement contains the breathing motion completely. For comparison, the respiratory motion measured by the reference system was also added to the figure.

V. Conclusion

This paper deals with the motion of a hovering UAV in six degrees of freedom. In particular, the effects of the motion on the detection of human targets as well as on the evaluation of the phase signals are analyzed. For each degree of freedom, an algorithm has been proposed to mitigate or even eliminate these effects. The capabilities of the algorithms were demonstrated by presenting realistic measurement results for each degree of freedom. Without the compensation the measurements were not usable at all. After compensation of the UAV motions with the proposed algorithms, the test person could be detected and the breathing motion in the extracted phase signals could be easily identified. The measured respiratory motions were validated against a vital sign reference system.

References

[1] R. H. Nakata, B. Haruna, T. Yamaguchi, V. M. Lubecke, S. Takayama, and K. Takaba, "Motion compensation for an unmanned aerial vehicle remote radar life sensor," *IEEE Journal on Emerging and Selected Topics in Circuits and Systems*, vol. 8, no. 2, pp. 329–337, 2018.

[2] R. Nakata, S. Clemens, A. Lee, and V. Lubecke, "Rf techniques for motion compensation of an unmanned aerial vehicle for remote radar life sensing," in *2016 IEEE MTT-S International Microwave Symposium (IMS)*, 2016, pp. 1–4.

[3] Y. Rong, A. Herschfelt, J. Holtom, and D. W. Bliss, "Cardiac and respiratory sensing from a hovering uav radar platform," in *2021 IEEE Statistical Signal Processing Workshop (SSP)*, 2021, pp. 541–545.

[4] J. Yan, Z. Peng, H. Hong, H. Chu, X. Zhu, and C. Li, "Vital-sar-imaging with a drone-based hybrid radar system," *IEEE Transactions on Microwave Theory and Techniques*, vol. 66, no. 12, pp. 5852–5862, 2018.

[5] S. Zhanshan, G. Min, and F. Yunqi, "Multiple targets 3d detection based on fmcw radar," in *2018 International Conference on Microwave and Millimeter Wave Technology (ICMMT)*, 2018, pp. 1–3.

[6] S. Rao, "Mimo radar - application report swra554a," Texas Instruments, Tech. Rep., May 2017. [Online]. Available: https://www.ti.com/lit/an/swra554a/swra554a.pdf?ts=1659900693914

[7] J. Wittemeier, A. M. Ahmed, T. N. Tran, A. Sezgin, and N. Pohl, "3d localization using a scalable fmcw mimo radar design," in *2020 German Microwave Conference (GeMiC)*, 2020, pp. 100–103.

[8] Y. Yuksel, N. El-Sheimy, and A. Noureldin, "Error modeling and characterization of environmental effects for low cost inertial mems units," in *IEEE/ION Position, Location and Navigation Symposium*, 2010, pp. 598–612.

[9] M. Kok, J. D. Hol, and T. B. Schoen, *Using Inertial Sensors for Position and Orientation Estimation*. Now Foundation and Trends, 2017.

[10] N. Anwar and M. Malik, "Antenna rotation effects and its compensation in radar signal processing," *Journal of Communications*, vol. 13, pp. 540–545, 09 2018.

[11] V. Lishchenko, H. Khudov, B. Lisogorsky, O. Baranik, D. Holovniak, and O. Serdjuk, "The mimo system on based existing mechanical rotation radars with wide surveillance area," in *2020 IEEE 40th International Conference on Electronics and Nanotechnology (ELNANO)*, 2020, pp. 625–628.

[12] L. Yanghuan, L. Fulai, S. Qian, and Z. Zhimin, "Lever arm rotation compensation method for uav mounted sar," in *2011 3rd International Asia-Pacific Conference on Synthetic Aperture Radar (APSAR)*, 2011, pp. 1–3.

[13] J. Yu, A. Dewantari, and M.-H. Ka, "Measurement of the rotation center from the received signals for ultrahigh-resolution radar imaging," *IEEE Antennas and Wireless Propagation Letters*, vol. 16, pp. 2266–2269, 2017.

[14] A. C. Bovik, "Chapter 3 - basic gray level image processing," in *The Essential Guide to Image Processing*, A. Bovik, Ed. Boston: Academic Press, 2009, pp. 43–68. [Online]. Available: https://www.sciencedirect.com/science/article/pii/B9780123744579000032

[15] Y. Rong, R. Gutierrez, K. V. Mishra, and D. W. Bliss, "Noncontact vital sign detection with uav-borne radars: An overview of recent advances," *IEEE Vehicular Technology Magazine*, vol. 16, no. 3, pp. 118–128, 2021.

[16] M. Stephan and A. Santra, "Radar-based human target detection using deep residual u-net for smart home applications," in *2019 18th IEEE International Conference On Machine Learning And Applications (ICMLA)*, 2019, pp. 175–182.

[17] *Evaluation module for integrated antenna-on-package (AoP) intelligent mmWave sensor*, Texas Instruments, May 2022, rev. G.

[18] *Intelligent mmWave sensor standard antenna plug-in module*, Texas Instruments, May 2022, rev. C.

[19] *Intelligent 9-axis absolute orientation sensor*, Bosch, October 2021, rev. 1.8.

[20] *HealthLab Satelliten-Master SAT-0M*, Koralewski Industrie - Elektronik HG —, August 2015.